DOI: 10.1002/cssc.201200817

Hydrothermal Carbons from Hemicellulose-Derived Aqueous Hydrolysis Products as Electrode Materials for Supercapacitors

Camillo Falco,*[a, b] Juan Manuel Sieben,[c] Nicolas Brun,[b] Marta Sevilla,[d] Torbjorn van der Mauelen,[e] Emilia Morallón,[c] Diego Cazorla-Amorós,[f] and Maria-Magdalena Titirici[b]

Acid pretreatment of lignocellulosic biomass, required for bioethanol production, generates large amounts of by-products, such as lignin and hydrolyzed hemicellulose fractions, which have found so far very limited applications. In this work, we demonstrate how the recovered hemicellulose hydrolysis products can be effectively utilized as a precursor for the synthesis of functional carbon materials through hydrothermal carbonization (HTC). The morphology and chemical structure of the synthesized HTC carbons are thoroughly characterized to highlight their similarities with glucose-derived HTC carbons. Furthermore, two routes for introducing porosity within the HTC carbon structure are presented: i) silica nanoparticle hard-templating, which is shown to be a viable method for the synthesis of carbonaceous hollow spheres; and ii) KOH chemical activation. The synthesized activated carbons (ACs) show an extremely high porosity (pore volume $\approx 1.0\ cm^3\,g^{-1}$) mostly composed of micropores (90% of total pore volume). Because of their favorable textural properties, the ACs are further tested as electrodes for supercapacitors, yielding very promising results ($300\ F\,g^{-1}$ at $250\ mA\,g^{-1}$) and confirming the high suitability of KOH-activated HTC carbons derived from spruce and corncob hydrolysis products as materials for electric double layer supercapacitors.

Introduction

The progressive depletion of fossil fuel resources and the need for carbon-neutral alternatives are increasingly fostering the research on biofuels. First-generation biofuels have been deemed to be an unfeasible long-term solution as they are in competition with the food supply chain. On the other hand, lignocellulosic biomass-derived biofuels bypass such a problem. For this reason, in the recent past they have been the subject of intense investigations, which have led to several positive developments towards their large-scale utilization.[1–6]

Ethanol production through cellulose-derived glucose microbial fermentation is certainly one of the most investigated biofuel synthesis routes. This biological conversion process requires as a first step either enzymatic or acid hydrolysis of the cellulosic substrate into its sugar building units. For this reason, lignocellulosic biomass is typically pretreated to make the cellulose fraction more accessible for the subsequent hydrolysis step. This can be accomplished by various techniques, such as steam or ammonia fiber explosion and hydrolysis using concentrated or diluted acids.[7–12]

All these methods generate considerable amounts of by-products, such as the isolated lignin fraction and hemicellulose-derived aqueous hydrolysis products. Together, these can account for approximately half of the starting feedstock mass depending on the type of biomass utilized. Despite their abundance, these by-products have so far found very limited use[13–18] as there are far less research efforts focusing on finding new possibilities for effective exploitation than on aiming at the development of new synthesis routes for cellulose-derived biofuels or on increasing the efficiency of existing biofuels. However, the effective utilization of these by-products is potentially crucial for the efficiency enhancement of the overall biomass-conversion process to value-added products and for the development of fully sustainable biorefinery schemes. For

[a] Dr. C. Falco
IASS - Institute for Advanced Sustainability Studies
BerlinerStrasse 130, 14467, Potsdam (Germany)
Fax: (+49) 331-288-22-404
E-mail: camillo.falco@iass-potsdam.de

[b] Dr. C. Falco, Dr. N. Brun, Dr. M.-M. Titirici
Colloid Chemistry, Max-Planck Institute for Colloids and Interfaces
Am Mühlenberg 1, 14476, Potsdam (Germany)

[c] Dr. J. M. Sieben, Prof. E. Morallón
Departamento de Química Física and Instituto Universitario de Materiales
Universidad de Alicante, Ap. 99 Alicante (Spain)

[d] Dr. M. Sevilla
Instituto Nacional del Carbón (CSIC)
P.O. Box 73, 33080 Oviedo (Spain)

[e] Dr. T. van der Mauelen
SEKAB E-Technology
PO Box 286, 891 26 Örnsköldsvik (Sweden)

[f] Prof. D. Cazorla-Amorós
Departamento de Química Inorgánica and
Instituto Universitario de Materiales
Universidad de Alicante, Ap. 99. Alicante (Spain)

Supporting Information for this article is available on the WWW under http://dx.doi.org/10.1002/cssc.201200817.

this reason, the aim of this study is to investigate the use of hemicellulose-derived aqueous hydrolysis products as potential carbon precursors for the hydrothermal carbonization (HTC) process aimed at the production of high-value functional carbon materials for energy storage applications (e.g., supercapacitors). The hemicellulose-derived by-products were generated during the dilute-acid pretreatment of lignocellulosic biomass (corncobs, spruce) in the cellulosic ethanol demonstration plant in Örnsköldsvik run by SEKAB (Sweden).

During the pretreatment step, the lignocellulosic biomass is impregnated with a diluted acid solution and heated by steam (Figure 1). At these processing conditions (i.e., high temperature, low pH), hemicellulose is readily hydrolyzed to monomeric carbohydrates. Exiting the reactor, the biomass-containing aqueous stream undergoes a rapid change of pressure leading to further disruption of the biomass fibrous structure and to the formation of a slurry-like effluent, which is then filtered to separate the solids (lignin and cellulose) from the aqueous phase. The latter contains predominantly carbohydrates originating from the biomass hemicellulose fraction. Depending on the biomass used, the filtrate composition may be characterized by slight variations (Table 1). Currently the main use of this by-product involves its fermentation to ethanol to increase the overall process yield. However, this process poses several challenges due to the fact that pentose-sugar fermentation requires a modified culture of yeast, the effectiveness of which can be very easily inhibited by other components present within the aqueous mixture [e.g., furfural, 5-hydroxymethylfurfural (5-HMF)].[19–21]

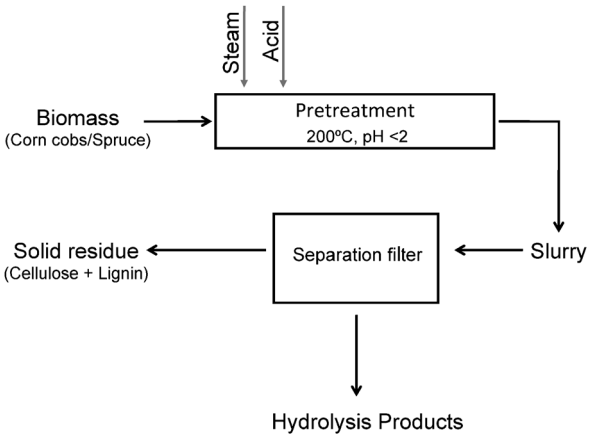

Figure 1. Flow diagram of the diluted-acid pretreatment unit at the cellulosic ethanol demonstration plant in Örnsköldsvik, Sweden.

Table 1. Composition of the hemicellulose-derived aqueous hydrolysis products obtained from diluted acid pretreatment of corncobs and spruce.

Component	Hydrolysis product [g L^{-1}]	
	corncobs	spruce
glucose	6.8	18.9
mannose	2.7	24.0
galactose	2.0	5.0
xylose	38.2	10.8
arabinose	5.1	3.9
acetic acid	4.7	4.9
5-hmf	0.5	3.4
furfural	1.6	2.6
levulinic acid	0	0.3

HTC has been demonstrated to be an effective synthetic route for the production of functional carbonaceous materials from simple monosaccharides, such as glucose and xylose.[22–27] As these sugars are the main components of the hydrolysis-product streams, it is foreseeable that these hemicellulose-derived by-products may be a suitable carbon precursor for the synthesis of high-value carbon-negative functional HTC materials. To confirm the feasibility of this hypothesis, this study compares the carbonaceous materials obtained from the hydrothermal treatment of the hemicellulose-derived hydrolysis products with those obtained from glucose HTC. Furthermore, it also shows the possibility of adopting hard-templating strategies or post-synthesis processing steps (e.g., KOH chemical activation) to obtain HTC carbon material with improved textural properties (e.g., specific ordered morphology, high surface area; Table 4). Promising preliminary results in relation to the use of the chemically activated HTC carbons as supercapacitors electrode materials are lastly presented, showing the effectiveness of this synthesis strategy in converting a low-value biomass-derived industrial by-product into a functional carbon material with evident energy storage applications.

Results and Discussion

The first part of this study focuses on the HTC of hydrolysis products derived from the diluted acid pretreatment of spruce and corncobs during ethanol production described above. The question whether such waste by-products are suitable precursors for the synthesis of hydrothermal carbon is addressed by comparing the carbonaceous materials obtained from hydrothermal treatment of these two feedstocks with those derived from glucose in terms of morphology and chemical structure. In the second part of this study the produced HTC carbons are chemically activated using KOH and then tested as electrode materials. Furthermore, a templating approach able to generate well-defined nano-sized hollow carbon spheres with controlled pore walls is also described. Such hollow spheres are promising candidates as electrodes materials in either Li^+, Na^+, or even Li–S batteries.[28–30]

Hemicellulose-derived by-product HTCs

SEM analysis reveals that the morphology of the HTC carbons, obtained from both spruce and corncob hydrolysis products, is characterized by interconnected microspheres (Figure 2a–d). This morphology is characteristic of monosaccharide-derived HTC carbons.[31] Hydrothermal carbonization of pure glucose (Figure 2e–f) yields a carbon composed of micrometer-sized spherical particles. However, in this latter case the average sphere diameter is smaller and the particle size distribution

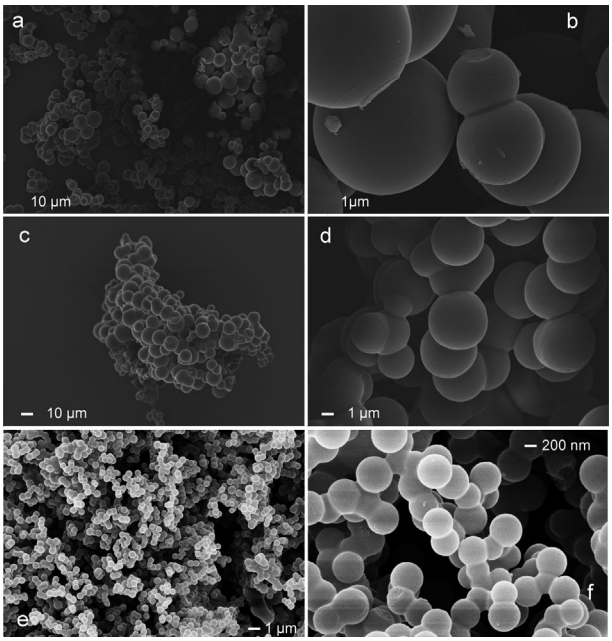

Figure 2. Scanning electron micrographs of hydrothermal carbon obtained from spruce hydrolysis product (a, b), corncob hydrolysis product (c, d), and glucose (e, f) at 200 °C and after 24 h.

narrower. A possible explanation for this observation is that the spruce and corncob hydrolysis products contain several different carbohydrates generated from hemicellulose hydrolysis (i.e., mannose, galactose, arabinose, xylose), which, as demonstrated by Titirici et al., affect the final particle size.[31]

Elemental analysis (EA) of the HTC carbons synthesized from both, hydrolysis products and pure glucose, shows very similar values (Table 2). This evidence suggests that the HTC of spruce and corncob hydrolysis products generates a carbonaceous material whose chemical composition and structure can be closely related to the one obtained from pure monosaccharides. Conversely, analysis of HTC yields underlines that this parameter varies considerably depending on the carbon precursor (Table 2). The HTC yields measured for the HTC carbons derived from spruce and corncob hydrolysis products are higher in comparison to those obtained for pure glucose. This difference is presumably caused by the presence of pentose sugars within the lignocellulosic-biomass hydrolysis products (Table 1), which are known to generate HTC carbon through dehydration to furfural.[31] Contrarily, 5-HMF is produced if glucose or generally hexoses are treated under hydrothermal conditions.[32] This latter reaction intermediate has a pronounced tendency to form degradation products (e.g., levulinic acid, formic acid, and dihydroxyacetone), especially under acidic conditions.[33,34] A higher extent of degradation-product formation of hexose sugars might be the cause of lower HTC yields. Further evidence for such a hypothesis is that the highest recorded yield corresponds to the HTC carbon obtained from corncob hydrolysis products, which is the feedstock with the largest fraction of pentose sugars (Table 1).

Table 2. Elemental composition and HTC yield of hydrothermal carbons obtained from spruce product and corncob hydrolysis product and glucose at 200 °C after 24 h.

HTC Sample	Elemental composition [wt%]					HTC yield
	H	C	O	N	S	[%]
spruce hydrolysis products	4.54	69.03	24.98	1.19	0.26	44.44
corncob hydrolysis products	4.55	70.36	23.50	1.43	0.16	51.36
glucose 200 °C	4.68	68.98	26.27	0.02	0.05	38.75

The ^{13}C solid-state NMR spectra of the HTC carbons obtained from all three carbon precursors show overall very similar features in all the NMR regions (carbonyl groups, aromatic, and aliphatic), which have been shown to be relevant for the analysis of the chemical structure of hydrothermal carbons (Figure 3).[35,36] This is the evidence that carbonaceous materials obtained from corncob and spruce hydrolysis products have the same chemical structure as the one obtained from glucose. However, some minor differences can still be found in the aromatic region of the spectra with a more focused analysis. Firstly, it can be observed that the HTC carbon derived from glucose at 200 °C already shows a well-developed arene-like aromatic structure: the most prominent peak in the aromatic region is the one at 125–128 ppm. This feature can be attributed to the processing temperature, which is high enough ($T >$ 180 °C) for the polyfuranic structure to be partially converted into a more aromatic one.[37] The same fingerprint applies also to the samples obtained from the two hydrolysis products. However, in the two latter cases the relative intensity of the central peak is even higher, especially for the corncob sample. This can be related to the presence of pentose sugars within the starting feedstocks, which have been shown to generate hydrothermal carbons with a higher aromatic character than those obtained from hexose sugars.[31]

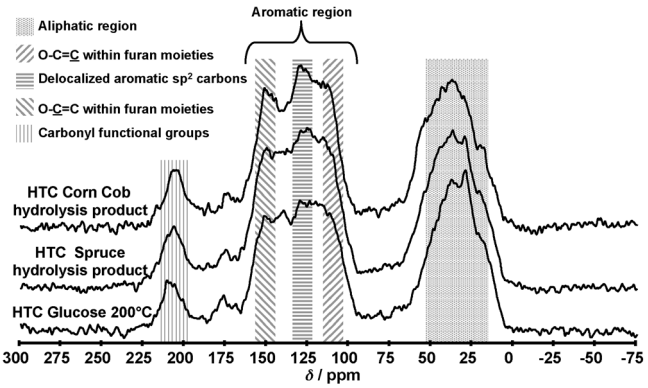

Figure 3. Solid state ^{13}C CP NMR spectra of hydrothermal carbon obtained from glucose, spruce, and corncob hydrolysis products at 200 °C and after 24 h.

FTIR analysis of all three hydrothermal carbons confirms the conclusions derived from the analysis of the NMR spectra. All profiles shown in Figure 4 are characterized by the same relevant peaks that highlight the presence of the same functional

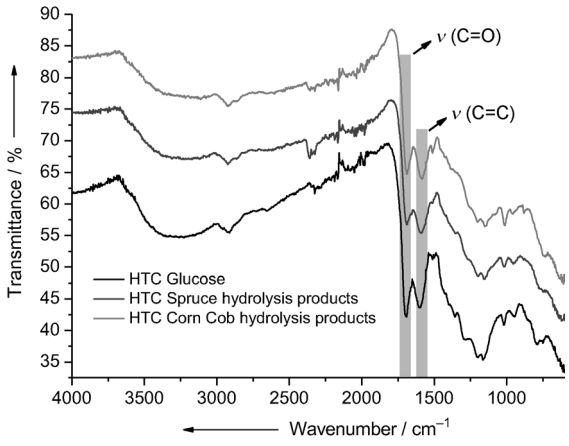

Figure 4. FTIR spectra of hydrothermal carbon obtained from glucose, spruce, and corncob hydrolysis products at 200 °C and after 24 h.

groups within all the obtained samples. However, one main difference can be observed. The ratio of the $\tilde{\nu}$(C=O) to the $\tilde{\nu}$(C=C) peaks is lower for the HTC carbons obtained from the hydrolysis products. A possible explanation might be that the pH value of these two sample solutions is lower because of the presence of H_2SO_4 remaining from the pretreatment stage. Therefore, the acid might enhance the degree of decarbonylation of the obtained HTC carbons, thus reducing the relative intensity of the carbonyl peak.

Introducing porosity in hydrolysis-product-derived HTC carbons

As generally observed for HTC carbons, the hydrolysis products have no relevant porosity, which hinders their potential utilization for energy storage applications. To introduce porosity within their structure, an attempt was made to obtain hollow spheres by templating silica nanoparticles. TEM micrographs of the HTC carbons replicating the silica particles show that the templating strategy represents a viable alternative to produce carbon hollow spheres (Figure 5). Tang et al. have recently demonstrated that HTC carbons, characterized by such morphology, show very promising performances as anode materials for Na and Li batteries.[28,29] As a consequence, it is possible that the templated hydrolysis-product-derived HTC carbons

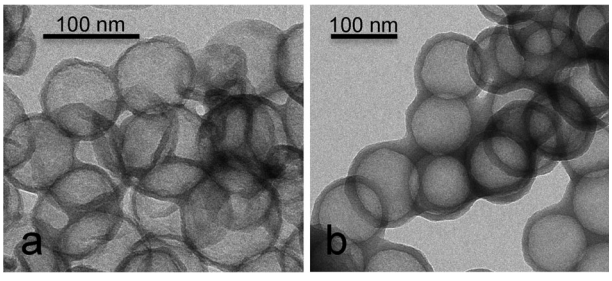

Figure 5. TEM micrographs of HTC carbons derived from hydrolysis products after using silica nanoparticles as templates: a) spruce, b) corncobs.

may be also successfully employed for such an end application.

KOH chemical activation was employed as a second synthesis strategy to introduce microporosity in hydrolysis-product-derived HTC carbons. SEM analysis reveals that the chemical activation process leads to a complete disruption of the morphology observed after HTC (Figure 6). The activated carbon

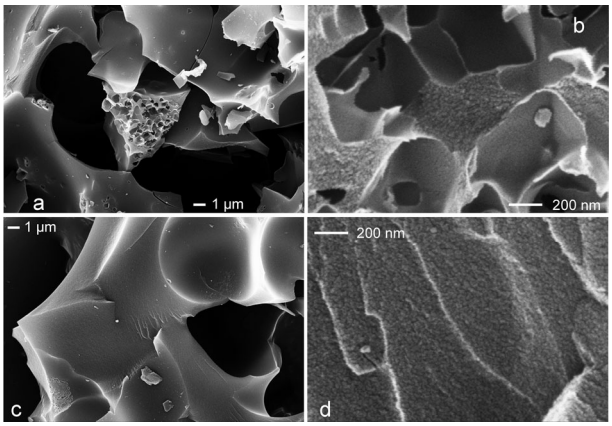

Figure 6. SEM micrographs of HTC carbons derived from hydrolysis products after chemical activation with KOH: a, b) spruce; c, d) corncobs.

(AC) materials are now composed of macrometer-sized monolithic fragments with sharp edges. Furthermore, higher magnification SEM micrographs show a high level of surface roughness, hinting at the material's extensive microporosity (Figure 6 b and d), which is also confirmed by high resolution SEM micrographs (SI2 in the Supporting Information). This complete morphological rearrangement suggests that the synthesis of ACs presumably proceeds via meltdown of the HTC carbon precursor and formation of a liquid-phase intermediate. Such observations are in agreement with the results reported for the chemical activation of carbonaceous precursors with a low degree of crystallinity.[38,39]

To fully characterize the porosity of the synthesized ACs, both CO_2 and N_2 gas adsorption were employed. The analysis was performed based on a combination of the Brunauer–Emmett–Teller (BET), and Dubinin–Radushkevich (DR), and DFT models applied to N_2 and CO_2 adsorption isotherms.

The N_2 isotherms of ACs produced from hydrolysis-product-derived HTC carbons are characterized by a Type I profile (Figure 7 a), exhibiting a sharp adsorption knee at low relative pressures, which is indicative of a narrow pore size distribution (PSD) and the essentially microporous nature of the adsorbents. The high N_2 volume uptakes reveal that KOH activation has effectively led to the development of extensive porosity within the carbon material structure. Such observations are confirmed by the calculated BET surface area and pore volume values (Table 3).

The comparison between the total pore volume and the micropore volume calculated from N_2 adsorption confirms that the samples are essentially microporous (Table 3). Additionally, the micropore volumes obtained from CO_2 adsorption reveal

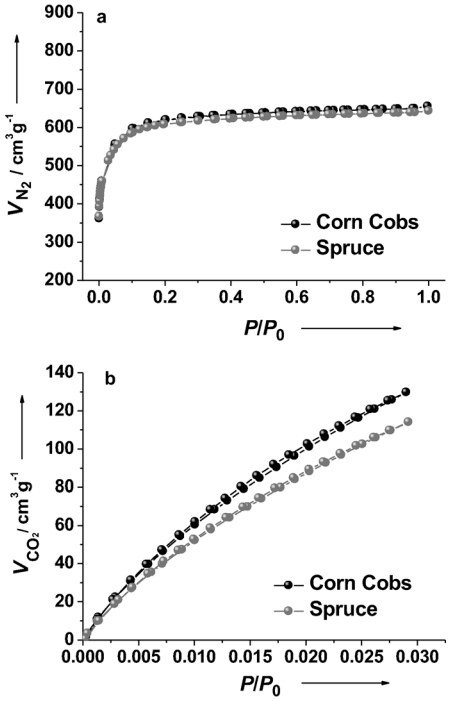

Figure 7. a) N_2 and b) CO_2 (at 273 K) adsorption isotherms of the ACs.

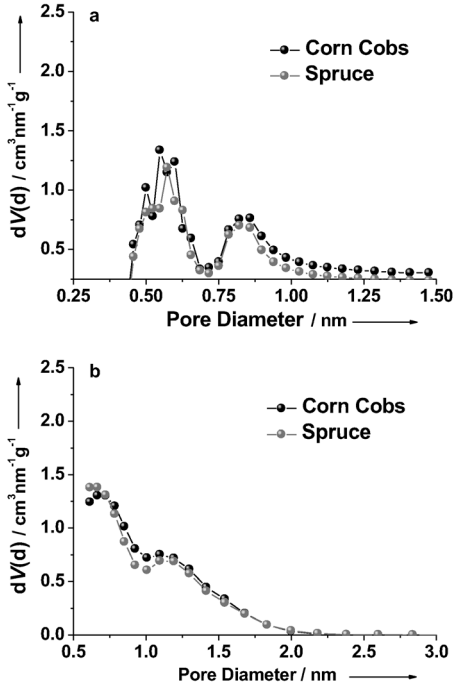

Figure 8. Pore size distributions obtained by applying the a) NLDFT method to CO_2 isotherms and b) QSDFT method to N_2 isotherms.

Table 3. Calculated surface area (*S*) and pore volume (*V*) using different models (subscript) on either N_2 or CO_2 isotherms for the ACs.

Sample	S_{BET} [m^2g^{-1}]	V_p [cm^3g^{-1}][a]	V_{N_2-DR} [cm^3g^{-1}]	V_{CO_2-DR} [cm^3g^{-1}]
spruce	2220	1.09	0.93	0.48
corncobs	2300	0.93	0.87	0.51

[a] The total pore volume was determined from the amount of nitrogen adsorbed at $p/p_o \approx 0.99$.

that the samples have a large fraction of narrow micropores (≈50–60% of total microporosity) (Figure 7b). The prevalent microporosity of both adsorbents is also confirmed by PSDs obtained with DFT methods that highlight the absence of relevant mesopore fraction (Figure 8a and b).

Electrochemical characterization.

It has been extensively demonstrated that a carbon material for electrochemical capacitors should exhibit good conductivity, high surface area, adequate PSD, excellent corrosion resistance, high thermal stability, and presence of electroactive species.[40,41] In this sense, the carbonaceous materials obtained by HTC treatment of biomass are expected to present good electronic conductivity.[42] Furthermore, chemical activation with KOH allows developing high surface areas and porosity prevalently composed of micropores (Table 3), even maintaining a relatively high content of nitrogen, oxygen, and sulfur in the carbon structures (Table SI2 in the Supporting Information).

Figure 9a shows the cyclic voltammograms (CVs) of the E1 and E2 electrodes (E1: AC from spruce hydrolysis-product-derived HTC carbon; E2: AC from corncob hydrolysis-product-derived HTC) obtained in a three electrode-cell in acidic medium. Both electrodes exhibit an almost rectangular shape, indicating that the main contribution to capacitance is the process involving the charging and discharging of the double layer. In addition, the voltammogram of the E2 electrode exhibits redox processes at around 0.65 V during the positive sweep and the counter peak at 0.45 V during the negative sweep; these are associated to surface oxygen groups. The specific capacitance (*C*) of E1 and E2 measured from the CVs curves is 261 (11.8 $\mu F\,cm^{-2}$ calculated using the BET surface area) and 291 $F\,g^{-1}$ (12.7 $\mu F\,cm^{-2}$), respectively. These values are comparable to those found for other advanced nanocarbon materials.[43]

In addition, galvanostatic experiments were used to measure the specific capacitance of both samples (Figure 9b). Capacitances were calculated according to $jt/\Delta E$, where j is the discharge current density per mass unit, t the discharge time, and ΔE the voltage window. Interestingly, these experiments show that E1 has a higher resistance than E2. As both of them have similar porous textures, these differences should be attributed to the different nanocrystalline structure. Figure 9c shows the variation of the specific capacitance as the gravimetric current density increases. It can be observed that the capacitance decreases for both carbon materials following a similar trend, with the capacitance of E2 remaining higher than that of E1 within the entire current range (25–1000 $mA\,g^{-1}$). The gradual loss of capacitance with current density is presumably related to the hindered or restricted diffusion of ions within small pores (ion-sieving effect), highlighting that the electrochemical double layer formation within the micropores becomes less

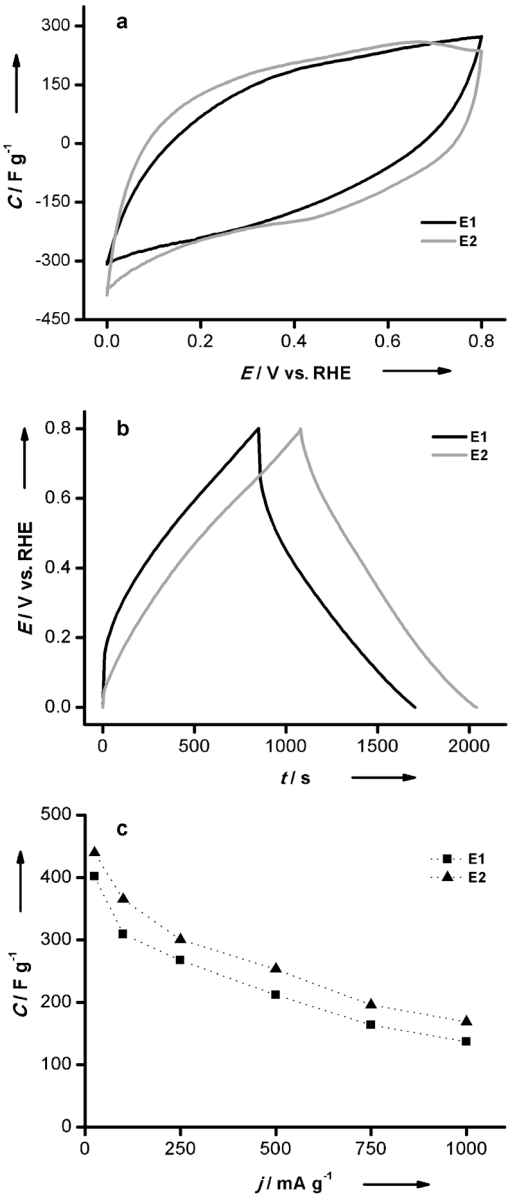

Figure 9. Electrochemical characterization using a three-electrode cell in 0.5 M H_2SO_4. a) CVs obtained at a scan rate of 1 mV s^{-1} . b) Galvanostatic curves at a current density of 250 mA g^{-1}. c) Variation of specific capacitance with increase of current density.

complete at progressively higher current densities.[44] The specific capacitances obtained from charge–discharge experiments at 250 mA g^{-1} are in good agreement with those obtained from CV experiments. Capacitances of 267 and 300 F g^{-1} were measured for electrodes E1and E2, respectively. As it is expected, the higher the surface area and the heteroatom content of the carbon material, the higher the specific capacitance.

Furthermore, both materials exhibit high capacitances in acidic media, which are very promising compared to other ACs with similar porosities.[45–47]

Although a three-electrode characterization is helpful for determining the electrochemical characteristics of a material, a two-electrode test cell provides the best indication of their performance as it reproduces the physical configuration, internal voltages, and charge transfer that occurs in a packaged supercapacitor.[48] In this respect, two-electrode cells with the same carbon material in both electrodes were assembled to evaluate the performance of the materials as electrodes in supercapacitors. The electrochemical characterization was the same used to evaluate the electrodes in a three-electrode cell. Figure 10a shows the charge–discharge curves obtained for

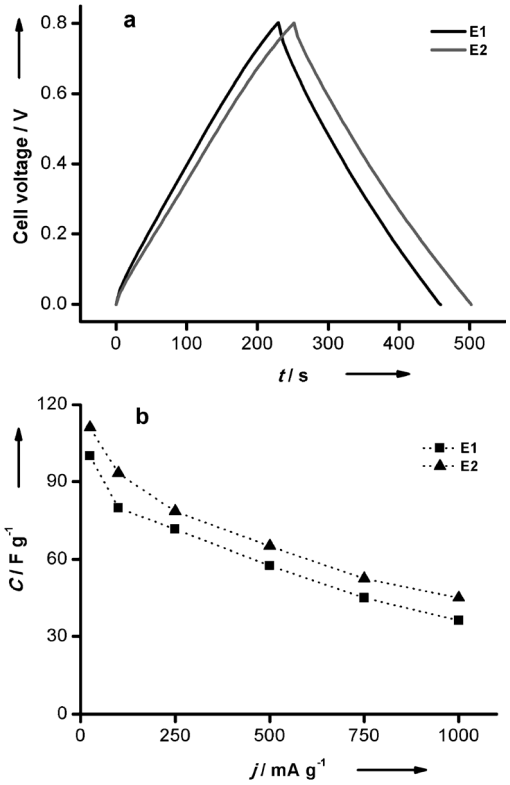

Figure 10. Electrochemical characterization using a two-electrode cell in 0.5 M H_2SO_4. a) Galvanostatic curves at a current density of 250 mA g^{-1}. b) Variation of specific capacitance with increase of current density.

both symmetric capacitors (E1/E1 and E2/E2) at a gravimetric current density of 250 mA g^{-1}, whereas the evolution of the capacitance with j is shown in Figures 10b, SI4, and SI5. The chronopotentiograms have a quasi-linear shape, and the coulombic efficiency is above 99%, which implies that no additional faradic reactions contribute significantly to the charge–discharge processes in the voltage window used.

In both capacitors the capacitances decrease similarly as the current density increases, and the capacitance of the symmetric E2/E2 capacitor is higher over the whole range of current densities.

In addition, it is important to remark that the specific capacitances determined from CV experiments at 1 mV s^{-1} (Figure SI4) are comparable to the values calculated from galvanostatic charge–discharge profiles at 250 mA g^{-1}.

To obtain a complete overview of the performance of the symmetric capacitors, the specific power and energy have been calculated according to the following expressions [Eqs. (1) and (2)]:

$$E = \frac{1}{2}CV^2 \quad (1)$$

$$P_{max} = \frac{V_{max}^2}{4 \cdot ESR \cdot m_t} \quad (2)$$

where *ESR* is the equivalent series resistance determined from the ohmic drop in the charge–discharge measurements and m_t is the total active mass of the capacitor.

A Ragone plot summarizes the performance of both capacitors over the whole current density range investigated in this work (Figure 11). For example, at 250 mA g^{-1} the symmetric capacitors E1/E1 and E2/E2 develop good energy densities, with values of 6.4 and 7 Wh kg^{-1}, respectively, and power densities of 0.76 and 1.08 kW kg^{-1} in the voltage window studied. These values confirm that the activated HTC carbons derived from spruce and corncob biomass are promising materials for electrical double layer supercapacitors (EDLCs), the performance of which could be further improved by tailoring the AC properties (e.g., PSD, heteroatom content) during the synthesis step.

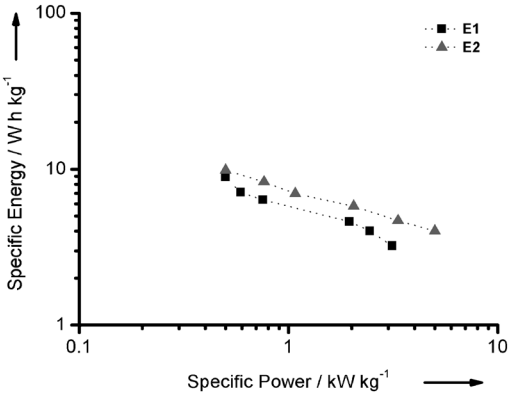

Figure 11. Ragone plot related to energy and power densities of samples E1 and E2 at a voltage window of 0.8 V (0–0.8 V).

Conclusions

In this study it has been shown how the HTC process allows exploiting a low-value by-product/waste of the bioethanol industry as a carbon precursor. Such feedstock can be used without any further pretreatment, therefore requiring a minimal increase in process complexity and contributing largely towards its intensification. The HTC carbons obtained from the corncob and spruce hydrolysis products have been demonstrated to exhibit comparable morphology and chemical nature as those obtained from pure monosaccharides (e.g., glucose). As a consequence, their use could be easily extended to the synthesis of nanostructured carbon materials, which have so far been synthesized from glucose through HTC adopting either hard/soft templating strategies or adding structure-directing agents. As a proof of concept, in this work the synthesis of carbon hollow spheres has been successfully demonstrated by using silica-nanoparticle templates.

To introduce porosity in the synthesized HTC carbons, KOH chemical activation has also been successfully exploited. It has been shown that the produced ACs exhibit an extremely high porosity (pore volume $\approx$ 1.0 cm^3 g^{-1}) mostly composed of micropores (90% of total pore volume). Because of their favorable textural properties, these materials have further been tested as electrodes for supercapacitors yielding very promising results (300 F g^{-1} at 250 mA g^{-1}). Such performances could be further improved by tailoring the AC properties (e.g., PSD, heteroatom content) during the synthesis step (i.e., controlling the activation-step variables).

Overall, the present work provides a remarkable contribution towards the implementation of the HTC process within industrial biorefinery schemes, as it shows how a readily available, high quantity, and low-value waste, generated during bioethanol production, can be effectively exploited as a precursor of HTC carbon materials, for which numerous applications have been reported within the available literature.

Experimental Section

HTC-carbon-derived AC Synthesis

Spruce and corncob hydrolysis products were produced at the cellulosic ethanol demonstration plant in Örnsköldsvik (Sweden) operated by SEKAB E-Technology. The composition of analysis was carried out by SEKAB E-technology by means of HPLC. Both hydrolysis products samples were HTC-treated at 200 °C for 24 h in a sealed autoclave equipped with a Teflon inlet.

After HTC treatment, the samples were filtered and washed with plenty of distilled water and then dried overnight in a vacuum oven at 80 °C. Chemical activation of both HTC carbons was then performed in a horizontal tubular oven using KOH as activating agent (Table 4). The ACs were thoroughly washed with 1 M HCl solution followed by a final distilled water wash.

Table 4. KOH activation parameters.

Parameter	Value
temperature	700 °C
heating rate	3 °C min^{-1}
holding time	1 h
KOH/carbon precursor ratio	4:1
mixing	physical

Synthesis of HTC carbon hollow spheres

Typically, 10 mL aqueous solutions containing amino-functionalized silica nanoparticles (Amino-NPs, 120 mg) and carbohydrate-equivalent hydrolysis products (0.3 mg) were prepared. After vigorous stirring for a few minutes, the solutions were then added in a glass inlet (30 mL volume) sealed in a Teflon-lined autoclave (45 mL volume) and placed in a laboratory oven preheated to the desired temperature (e.g., 180 °C) and left for the desired reaction time (e.g., 20 h). The powders obtained were then removed from the glass inlets and successively centrifuged and washed a few times in water and absolute ethanol to remove the residual unreacted precursors and by-products. The carbon-coated silica-based nano-

particles were then placed in a ceramic crucible in a carbonization oven and heated to the desired temperature (e.g., 950 °C) under an inert atmosphere (i.e., N_2 at a flow rate of 10 mL min^{-1}). The following heating program was used: a first ramp to reach 350 °C at a speed of 5 °C min^{-1}, a second ramp to reach 950 °C at 2 °C min^{-1} and an isothermal step of 2 h. Samples were then allowed to cool to ambient conditions, removed from the oven, and washed twice overnight in a solution of ammonium hydrogen difluoride (4 mol%) to remove the silica template. The as-synthesized hollow spheres were then washed in distilled water and dried overnight.

Characterization of HTC carbons

Elemental Analysis (EA) was performed by using an Elementar vario MICRO cube. SEM images were acquired using a LEO 1550/LEO GmbH Oberkochen equipped with an Everhard Thornley secondary electron and in-lens detectors. FTIR spectra of the materials were recorded in attenuated total reflectance (ATR) geometry on a Varian 1000 FTIR spectrometer, Scimitar Series (FTS1000). ^{13}C solid-state magic angle spinning (MAS) NMR spectra were acquired by using a Bruker Avance 300 MHz (7 T) spectrometer using 4 mm zirconia rotors as sample holders, spinning at MAS rate $n_{MAS} = 14$ kHz. The chemical shift reference was tetramethylsilane (TMS; $\delta = 0$ ppm).The ^1H t_1 relaxation time was set to 3 s. Proton-to-carbon cross polarization (CP) MAS was used to enhance carbon sensitivity by using a CP time equal to 1 ms.

Porosity Characterization

The characterization of the porous texture was assessed by performing gas adsorption experiments, N_2 (77 K) and CO_2 (273 K) adsorption, in a QUADRASORB SI apparatus equipped with an automated surface-area and pore-size analyzer. The specific surface area and the micropore volume were calculated by fitting nitrogen adsorption data to BET and DR equation, respectively.[49] Narrow micropore volume (mean pore size lower than about 0.7 nm) was obtained by fitting DR equation to CO_2 isotherm data. PSDs were evaluated from both adsorptive by using the quenched solid-state density functional theory (QSDFT) method for N_2 and the non-local density functional theory (NLDFT) method for CO_2 (QUADRAWIN software). TEM was carried out by using a Carl Zeiss Omega 912X at an acceleration voltage of 120 kV.

Electrochemical experiments

Suprapure sulfuric acid was purchased from Merck, acetylene black from Strem Chemicals, and the binder (polytetrafluoroethylene, PTFE) from Sigma–Aldrich. The electrolyte solution was prepared with purified water obtained from an Elga Labwater Purelab system (18.2 MΩ cm).

For the electrode preparation, the carbon materials were mixed with the binder PTFE (60 wt%) and acetylene black (Strem Chemicals) in a ratio 80:10:10 (wt%). The materials were mixed and pressed up to 1 ton for 10 min. The total electrode weight (HTC carbon, binder, and acetylene black) used for the measurements in the three-electrode cell was about 40 mg. After that, the electrode was placed on a stainless steel mesh (1 cm width and 6 cm height), which was used as current collector, by pressing the electrode onto the mesh under 1 ton for 10 min.

The electrochemical characterization of the electrodes was performed by using a standard three-electrode cell configuration. The counter electrode was a platinum wire, and a reversible hydrogen electrode (RHE) served as reference. All potentials mentioned in this work are referred to this electrode. An inert nitrogen atmosphere was maintained over the electrolyte. An aqueous electrolyte solution of 0.5 M H_2SO_4 was used. The measurements were carried out with an EG&G Potentiostat/Galvanostat model 273 and an Autolab PGSTAT302. The electrochemical behavior of the samples was assessed by CV at 1 mV s^{-1} and galvanostatic charge–discharge experiments. Capacitances were calculated from the scanning range between 0 and 0.8 V by dividing the imposed current with the slope of the linear chronopotentiograms plot, taking the average value between charge and discharge processes. The capacitance is expressed in F g^{-1} taking into account the weight of the active part of the electrode.

Experiments were also performed in a two-electrode cell using a sandwich-type construction (electrode/separator/electrode) with a nylon membrane (0.45 μm pore size) between the electrodes. Gold was used as the current collector and a 0.5 M H_2SO_4 solution as the electrolyte. Electrode discs with 10 mm diameter and about 0.25 mm thickness were cut from carbon pastes. The values of specific capacitances of the two-electrode cell were determined by galvanostatic charge–discharge measurements at different current densities and CV at 1 mV s^{-1}. *ESR* was calculated from the voltage drop (ΔV) observed in the discharge curve according to $\Delta V = I \times ESR$.

Acknowledgements

The authors would like to thank SEKAB for making the hydrolysis product samples available and, therefore, for allowing the development of the work presented within this manuscript. The technical staff of the Colloids department at the Max Planck Institute of Colloids and Interfaces is thanked for all the help provided with analytical measurements. The Laboratoire de Chimie de la Matiere Condensee de Paris Centre 'and especially Dr. Niki Baccile, Prof. Florence Babonneau, and Ing. Guillaume Laurent are thanked for their help and assistance during NMR measurements. C.F. thanks Dr. Luca Bertinetti for the help provided with high-resolution SEM measurements. Financial support by the Ministerio de Ciencia e Innovación (MAT2010-15273 and CTQ2009-10813) and Generalitat Valenciana and FEDER (PROMETEO/2009/047 and ACOMP2012/133) projects are gratefully acknowledged. J.M.S. thanks Ministerio de Educación (SB2010-132).

Keywords: biomass · carbon · green chemistry · microporous materials · supercapacitors

[1] G. W. Huber, S. Iborra, A. Corma, *Chem. Rev.* **2006**, *106*, 4044.
[2] J. N. Chheda, G. W. Huber, J. A. Dumesic, *Angew. Chem.* **2007**, *119*, 7298; *Angew. Chem. Int. Ed.* **2007**, *46*, 7164.
[3] R. Palkovits, *Angew. Chem.* **2010**, *122*, 4434; *Angew. Chem. Int. Ed.* **2010**, *49*, 4336.
[4] M. Stöcker, *Angew. Chem.* **2008**, *120*, 9340; *Angew. Chem. Int. Ed.* **2008**, *47*, 9200.
[5] A. A. Peterson, F. Vogel, R. P. Lachance, M. Froling, M. J. Antal, J. W. Tester, *Energy Environ. Sci.* **2008**, *1*, 32.
[6] K. Tajvidi, K. Pupovac, M. Kukrek, R. Palkovits, *ChemSusChem* **2012**, *5*, 2139 – 2142.
[7] P. Kumar, D. M. Barrett, M. J. Delwiche, P. Stroeve, *Ind. Eng. Chem. Res.* **2009**, *48*, 3713.
[8] J. C. Serrano-Ruiz, J. A. Dumesic, *Energy Environ. Sci.* **2011**, *4*, 83 – 99.
[9] B. Yang, C. E. Wyman, *Biofuels Bioprod. Biorefin.* **2008**, *2*, 26.
[10] A. T. W. M. Hendriks, G. Zeeman, *Bioresour. Technol.* **2009**, *100*, 10.

[11] M. W. Lau, C. Gunawan, B. E. Dale, *Biotechnol. Biofuels* **2009**, *2*, 30.
[12] N. Kuzhiyil, D. Dalluge, X. Bai, K. Ho Kim, R. C. Brown, *ChemSusChem* **2012**, *5*, 2228.
[13] J. H. Lora, W. G. Glasser, *J. Polym. Environ.* **2002**, *10*, 39.
[14] W. Thielemans, E. Can, S. S. Morye, R. P. Wool, *J. Appl. Polym. Sci.* **2002**, *83*, 323.
[15] Suhas, P. J. M. Carrott, M. M. L. R. Carrott, *Bioresour. Technol.* **2007**, *98*, 2301.
[16] J. Hayashi, A. Kazehaya, K. Muroyama, A. O. Watkinson, *Carbon* **2000**, *38*, 1873.
[17] R. Xing, A. V. Subrahmanyam, H. Olcay, W. Oi, G. P. van Walsum, H. Pendse, G. W. Huber, *Green Chem.* **2010**, *12*, 1933.
[18] R. Xing, W. Oi, G. W. Huber, *Energy Environ. Sci.* **2011**, *4*, 2193.
[19] S. Walton, A. van Heiningen, P. van Walsum, *Bioresour. Technol.* **2010**, *101*, 1935.
[20] L. O. Ingram, H. C. Aldrich, A. C. C. Borges, T. B. Causey, A. Martinez, F. Morales, A. Saleh, S. A. Underwood, L. P. Yomano, S. W. York, J. Zaldivar, S. D. Zhou, *Biotechnol. Prog.* **1999**, *15*, 855.
[21] J. R. M. Almeida, D. Runquist, V. S. I. Nogue, G. Liden, M. F. Gorwa-Grauslund, *Biotechnol. J.* **2011**, *6*, 286.
[22] M. M. Titirici, M. Antonietti, *Chem. Soc. Rev.* **2010**, *39*, 103.
[23] B. Hu, K. Wang, L. Wu, S.-H. Yu, M. Antonietti, M.-M. Titirici, *Adv. Mater.* **2010**, *22*, 813.
[24] M. Antonietti, M. M. Titirici, *C. R. Chim.* **2010**, *13*, 167.
[25] R. J. White, N. Yoshizawa, M. Antonietti, M. M. Titirici, *Green. Chem.* **2011**, DOI: 10.1039/c1gc15349h.
[26] M. Sevilla, A. B. Fuertes, *Energy Environ. Sci.* **2011**, *4*, 1765.
[27] M. Sevilla, A. B. Fuertes, R. Mokaya, *Energy Environ. Sci.* **2011**, *4*, 1400.
[28] K. Tang, L. Fu, R. J. White, L. Yu, M. M. Titirici, M. Antonietti, J. Maier, *Adv. Energy Mater.* **2012**, *2*, 873 – 877.
[29] K. Tang, R. J. White, X. Mu, M. M. Titirici, P. A. van Aken, J. Maier, *ChemSusChem* **2012**, *5*, 400 – 403.
[30] X. Lai, J. E. Halpert, D. Wang, *Energy Environ. Sci.* **2012**, *5*, 5604.
[31] M. M. Titirici, M. Antonietti, N. Baccile, *Green Chem.* **2008**, *10*, 1204 – 1212.
[32] A. Gandini, M. N. Belgacem, *Prog. Polym. Sci.* **1997**, *22*, 1203 – 1379.
[33] M. Möller, P. Nilges, F. Harnisch, U. Schröder, *ChemSusChem* **2011**, *4*, 566 – 579.
[34] N. S. Mosier, C. M. Ladisch, M. R. Ladisch, *Biotechnol. Bioeng.* **2002**, *79*, 610 – 618.
[35] N. Baccile, G. Laurent, F. Babonneau, F. Fayon, M.-M. Titirici, M. Antonietti, *J. Phys. Chem. C* **2009**, *113*, 9644 – 9654.
[36] C. Falco, F. Perez Caballero, F. Babonneau, C. Gervais, G. Laurent, M.-M. Titirici, N. Baccile, *Langmuir* **2011**, *27*, 14460 – 14471.
[37] C. Falco, N. Baccile, M.-M. Titirici, *Green Chem.* **2011**, *13*, 3273 – 3281.
[38] M. A. Lillo-Ródenas, J. Juan-Juan, D. Cazorla-Amoros, A. Linares-Solano, *Carbon* **2004**, *42*, 1371.
[39] M. Sevilla, C. Falco, M. M. Titirici, A. B. Fuertes, *RSC Adv.* **2012**, *2*, 12792 – 12797.
[40] S. Bose, T. Kuila, A. K. Mishra, R. Rajasekar, N. H. Kim, J. K. Lee, *J. Mater. Chem.* **2012**, *22*, 767 – 784.
[41] E. Frackowiak, F. Béguin, *Carbon* **2001**, *39*, 937 – 950.
[42] L. Zhao, N. Baccile, S. Gross, Y. Zhang, W. Wei, Y. Sun, M. Antonietti, M. M. Titirici, *Carbon* **2010**, *48*, 3778 – 3787.
[43] M. Inagaki, H. Konno, O. Tanaike, *J. Power Sources* **2010**, *195*, 7880 – 7903.
[44] A. G. Pandolfo, A. F. Hollenkamp, *J. Power Sources* **2006**, *157*, 11 – 27.
[45] M. J. Bleda-Martínez, J. A. Maciá-Agulló, D. Lozano-Castelló, E. Morallón, D. Cazorla-Amorós, A. Linares-Solano, *Carbon* **2005**, *43*, 2677 – 2684.
[46] M. Kawaguchi, T. Yamanaka, Y. Hayashi, H. Oda, *J. Electrochem. Soc.* **2010**, *157*, A35 – A40.
[47] O. Barbieri, M. Hahn, A. Herzog, R. Kötz, *Carbon* **2005**, *43*, 1303 – 1310.
[48] M. D. Stoller, R. S. Ruoff, *Energy Environ. Sci.* **2010**, *3*, 1294 – 1301.
[49] D. Cazorla-Amorós, J. Alcaniz-Monge, M. A. Casa-Lillo, A. Linares Solano, *Langmuir* **1998**, *14*, 4589.

Received: October 29, 2012
Published online on January 14, 2013